THE ASTROPHYSICAL JOURNAL, 385:244–254, 1992 January 20


# THE MOLECULAR CORE IN G34.3+0.2: MILLIMETER INTERFEROMETRIC OBSERVATIONS OF $HCO^+$, $H^{13}CN$, $HC^{15}N$, AND SO

PATRICIA CARRAL[1]
Radio Astronomy Laboratory, University of California at Berkeley; and Space Science Division, NASA/Ames Research Center
AND
WILLIAM J. WELCH[2]
Radio Astronomy Laboratory, University of California at Berkeley
*Received 1991 May 17; accepted 1991 July 22*

## ABSTRACT

High-resolution observations of the molecular core in the star-forming region G34.3+0.2 are presented. Maps at 6″ resolution of emission and absorption of the $J = 1 \rightarrow 0$ transitions of $HCO^+$, $H^{13}CN$, $HC^{15}N$, and of the $2_2 \rightarrow 1_1$ transition of SO were obtained in addition to a map of the 3.4 mm continuum emission from the compact H II component.

The $HCO^+$ emission toward G34.3+0.2 traces a warm ($T_K \gtrsim 25$ K) molecular core about 0.9 pc in size. Emission from $H^{13}CN$ is detected over $\sim$0.3 pc. The cometary H II region lies near the edge of the molecular core. The location of the H II region in the core combined with the fact that the radio recombination lines are blueshifted with respect to the molecular emission suggests that ionized gas from the H II region is accelerated in a champagne flow caused by a steep gradient in the ambient gas density. A velocity gradient of $\sim 5 \pm 1$ km s$^{-1}$ pc$^{-1}$, consistent with rotation, is detected across the $HCO^+$ molecular core. The position angle of the rotation axes is $110° \pm 25°$.

The SO and $HC^{15}N$ emissions detected in G34.3+0.2 originate in a small region ($\lesssim$0.07 pc) located at the eastern edge of the compact H II region. The SO and HCN fractional abundances in this source appear to be locally enhanced. The compact SO source, high-velocity $H_2O$ masers in the region as well as the abundance enhancements may be associated with an outflow source produced by a young obscured object. A velocity gradient $\sim 20 \pm 10$ km s$^{-1}$ pc$^{-1}$ is detected across the compact source. The velocity gradient could be associated with an expanding and/or rotating flattened structure.

Three absorption features were detected against the compact continuum source in the $HCO^+$ spectrum. Two of them, at velocities of 27 and 52 km s$^{-1}$, appear to be foreground clouds along the line of sight not associated with the dense $HCO^+$ core. The third component, at 61 km s$^{-1}$, is redshifted with respect to the core LSR velocity of $\sim$57 km s$^{-1}$ and is apparently associated with the core. The 61 km s$^{-1}$ absorbing gas may be part of an envelope surrounding the warm core and collapsing upon it, or alternatively, a foreground cloud moving toward the dense core and probably interacting with it.

*Subject headings:* H II regions — ISM: abundances — ISM: individual (G34.3+0.2) — radio lines: molecular: interstellar — stars: formation

## 1. INTRODUCTION

The H II region complex G34.3+0.2 lies 3.8 kpc away from the Sun. High-resolution radio continuum maps resolve the H II complex into one compact ($\sim 4'' \times 20''$) and two ultracompact ($\sim$0.″3) components (see, e.g., Reid & Ho 1985). Reid & Ho describe the morphology of the compact H II region by analogy with comets; it has a bright compact "head" approximately 4″ ($\sim$0.07 pc) in size and a 20″ (0.37 pc) "tail" trailing to the west. They argue that this peculiar shape may be the consequence of a relative motion between the star and the molecular gas. Alternatively, Garay, Rodríguez, & van Gorkom (1986, hereafter GRvG) suggest that the radio morphology could be understood if the H II region is going through a "champagne" phase.

The ionized gas in the cometary H II region shows peculiar kinematics. First, the radio recombination lines are unusually broad (FWHM $\sim$ 50 km s$^{-1}$). The width cannot be easily understood as a combination of thermal broadening plus the usual turbulent motions observed in normal H II regions ($v_t \leq$ 15 km s$^{-1}$), and neither as pressure broadening (GRvG). Second, high-resolution (0.″4) observations of the radio recombination line H76α emission by GRvG show a very large velocity shift ($\sim$23 km s$^{-1}$) of the line peak across the compact component.

Maser emission of $H_2O$ and OH has been detected close to the H II region. The $H_2O$ emission is seen over the velocity range 45–85 km s$^{-1}$ (Downes et al. 1979), while the OH masers have velocities from $\sim$56 to 63 km s$^{-1}$ (Gaume & Mutel 1987). The velocity centroid of the OH maser emission has a large ($\gtrsim$10 km s$^{-1}$) redshift with respect to the $\sim$46 km s$^{-1}$ mean radial velocity of the H66α radio recombination line (Garay, Reid, & Moran 1985). The LSR velocity of the H41α radio recombination line at $\nu = 92$ GHz, $V_{LSR} = 48.8 \pm 1.4$ km s$^{-1}$ (Forster et al. 1990), is also blueshifted $\sim$8 km s$^{-1}$ with respect to the OH masers and other molecular lines with $V_{LSR} \sim$ 57–59 km s$^{-1}$.

Single-dish $NH_3$ maps toward G34.3+0.2 obtained by Heaton et al. (1985) with 2.′2 and 40″ resolution trace an extended ($\sim 3.4 \times 4$ pc) "halo" with density $n(H_2) \sim 6 \times 10^3$

[1] Postal address: NASA/Ames Research Center, Mail Stop 245–6, Moffett Field, CA 94035.
[2] Postal address: University of California, Radio Astronomy Laboratory, Berkeley, CA 94720.

$cm^{-3}$ surrounding a $\sim 1.7$ pc denser "core" [$n(H_2) \sim 3 \times 10^4$ $cm^{-3}$]. Observations of $H_2CO$ and $CH_3CN$ by Martín-Pintado et al. (1985) and Andersson (1985) suggested that dense molecular structures [$n(H_2) > 10^4$–$10^5$ $cm^{-3}$] exist within the core. Matthews et al. (1987) obtained single-dish maps of the region in rotational transitions of $HCO^+$, $^{13}CO$, and $^{12}CO$. From their data they infer the presence of dense [$n(H_2) \sim 10^6$ $cm^{-3}$] condensations in the core, and a total cloud mass $> 10^3$ $M_\odot$. They detected redshifted self-absorbed profiles which they attribute to absorption by a tenuous [$n(H_2) \sim 2$–$3 \times 10^3$ $cm^{-3}$] foreground cloud with temperature $T_{ex}(CO) = 9$ K.

At high resolution, the velocity structure of the molecular core has been investigated by Carral, Welch, & Wright (1987) and Keto, Ho, & Reid (1987b). Keto et al. (1987b) interpret the kinematics as a combination of rotation and infall of the massive core toward the compact H II region. Andersson & Garay (1986, hereafter AG) observed the (3, 3) inversion line of ammonia with $6'' \times 3''$ resolution and detected a dense, warm ($T_K = 60$ K) elongated "compact core" ($0.21 \times 0.05$ pc) located close to the "head" component of the compact H II region. With better resolution (1".4), Heaton, Little, & Bishop (1989, hereafter HLB) find a smaller molecular component, the "ultracompact core" (size $0.06 \times \lesssim 0.02$ pc), which lies to the side of the H II region. They infer a mass $\sim 170$ $M_\odot$, assuming the core is in virial equilibrium, which implies a mean density $n(H_2) \sim 4 \times 10^7$ $cm^{-3}$. Garay & Rodríguez (1990, hereafter GR) made 3" VLA observations of the (2, 2) and (3, 3) ammonia lines obtaining a rotational temperature in the ultracompact core of 185 K and a density of $\sim 7 \times 10^7$ $cm^{-3}$. Henkel, Wilson, & Mauersberger (1987, hereafter HWM) detected 15 $NH_3$ inversion transitions toward the compact core using the Effelsberg 100 m telescope. They first detected the ultracompact core and measured a rotational temperature $T_{rot} = 225 \pm 75$ K and a hydrogen column density $N(H_2) = 10^{23.6 \pm 0.1}$ $cm^{-2}$ for the region. The derived column density for this ultracompact core is similar to or even larger than that derived for the "hot core" in Orion KL.

In this paper we investigate the mass distribution, kinematics, and chemical abundances of the molecular core associated with G34.3+0.2 by looking at the emission from various molecular species with high spatial resolution ($\sim 6''$). We chose to look at the $J = 1 \rightarrow 0$ rotational transitions of $HCO^+$, $H^{13}CN$, and $HC^{15}N$, and the $(2_2 \rightarrow 1_1)$ transition of SO. The molecule $HCO^+$ is abundant in molecular clouds and therefore is a good tracer of extended, dense [$n(H_2) \gtrsim 4 \times 10^4$ $cm^{-3}$] gas. The $H^{13}CN$ and $HC^{15}N$ isotopes of HCN are less abundant and therefore are good indicators of regions with high column density. SO appears to be enhanced near outflow sources (Welch 1988) and therefore provides a probe of outflow activity in G34.3+0.2. The SO, $H^{13}CN$, and $HC^{15}N$ transitions require high densities to be excited and thus are also good tracers of dense gas. In § 2, we describe the observations and in § 3 the results. We present a discussion of the models for the region in § 4 and the conclusions in § 5.

## 2. OBSERVATIONS

The observations were made with the BIMA–Hat Creek millimeter array. The source G34.3+0.2, located at $\alpha = 18^h50^m46^s.14$ and $\delta = 01°11'12''.5$, was observed from 1985 November to 1986 June. The source was observed in a total of seven antenna configurations (21 baselines) which gave a maximum projected baseline of 95 m. The flexibility of the correlator at Hat Creek allowed us to observe simultaneously, the $HCO^+(J = 1 \rightarrow 0)$ rotational transition in the upper sideband and the SO $(2_2 \rightarrow 1_1)$, $H^{13}CN(J = 1 \rightarrow 0)$ and $HC^{15}N(J = 1 \rightarrow 0)$ transitions in the lower sideband. The correlator was set to assign 64 channels to each of the chosen IF bands. We used 20 MHz bandwidths, obtaining a velocity coverage of 67 km $s^{-1}$ and a channel width of 1.05 km $s^{-1}$ at 89 GHz. On-line Hanning-smoothing was applied to the data, giving an effective spectral resolution of 2.1 km $s^{-1}$.

The quasars 1749+07 and 3C 454 were used as calibrators to correct for instrumental phase variations with time. The source was observed in 30 minute intervals, followed by 10 min integrations on the calibrator. The quasars were observed with a total IF bandwidth of 320 MHz to obtain maximum signal-to-noise ratio. System temperatures ranged from 300–900 K SSB scaled above the atmosphere. The absolute flux calibration was done scaling to the flux measured for 3C 454 relative to Mars. The uncertainty in the absolute flux calibration is about 30%. The instrumental passband shape was measured from observations of Venus at short baselines and 3C 273, otherwise.

The data reduction was done using the Hat Creek reduction package. Channel maps for the four lines observed were obtained with both uniform and natural weighting of the data. A continuum map at 3.4 mm was produced averaging the data from the three 20 MHz windows in the upper sideband free of spectral lines. CLEANed channel maps were made for the line plus continuum emission and also for line emission only. The continuum subtraction was done before the CLEANing. For the lines in the lower sideband, the subtracted continuum map was made from a 20 MHz line-free section of the passband. The CLEAN beam size and the noise measured in individual channel maps are shown on Table 1. The parameters measured for the continuum map are also indicated.

## 3. RESULTS

### 3.1. *Radio Continuum Emission at 3.4 Millimeters*

The radio continuum emission at 3.4 mm toward G34.3+0.2 was mapped with a spatial resolution of $6''.3 \times 5''.6$. The compact head of the H II region is unresolved in our map, and the peak flux measured is 5.4 Jy $beam^{-1}$. A slightly extended component is also present as indicated by the apparent size of the continuum source ($\sim 7''.5 \times 6''.3$) compared to the size of our beam. The total measured flux in the map is 8 Jy. The extended component is probably a combination of free-free emission produced in the tail of the cometary H II region and thermal dust emission. Chini, Krügel, & Wargau (1987) measured a flux of 27.4 Jy at 1.3 mm in a 90" beam. If the flux at 1.3 mm is mostly due to thermal radiation from dust, we estimate an upper limit of 1.6 Jy for the 3 mm dust emission flux

TABLE 1

G34.3+0.2 MAP PARAMETERS

| Emission | Weight | Beam Size | Beam P.A. | RMS Noise[a] (K) |
|---|---|---|---|---|
| $HCO^+$ ..... | Uniform | $6''.3 \times 5''.6$ | 83° | 1.3 |
| $H^{13}CN$ ..... | Uniform | $6.5 \times 5.4$ | 90 | 1.2 |
| SO ..... | Uniform | $6.5 \times 5.4$ | 90 | 1.1 |
| $HC^{15}N$ ..... | Natural | $8.3 \times 6.9$ | 153 | 0.6 |
| 3.4 mm ..... | Uniform | $6.3 \times 5.6$ | 83 | 0.4 |

[a] For the molecular lines, the noise refers to individual channel maps.

expected in G34.3+0.2 assuming a dust opacity proportional to $\lambda^{-1}$ (see, e.g., Wright & Vogel 1985). The dependence of the dust opacity on wavelength is uncertain, but measured values for the exponent vary mostly between $-1$ and $-2$. A dust opacity with an exponent equal to $-2$ would give 0.6 Jy for the 3.4 mm dust emitted flux predicted from the value measured at 1.3 mm. We expect therefore that at least 6.4 Jy of the flux we observed at 3.4 mm originates as free-free emission from the compact H II region.

The compact H II region G34.3+0.2 has been previously observed at radio frequencies from 1.6 to 43 GHz. To derive the physical parameters of the ionized gas we fitted the radio spectrum observed toward G34.3+0.2 with the theoretical spectrum of a homogeneous H II region. We used the expressions for the optical depth and continuum flux given by GRvG. The free parameters in the fit are the average emission measure (EM) along the line of sight and the effective blackbody area ($A_{BB}$) of the ionized gas. We assumed the electron temperature in the region is $10^4$ K and used a distance to the source of 3.8 kpc. The radio fluxes measured toward G34.3+0.2 at frequencies from 1.6 to 89 GHz are plotted in Figure 1. The solid line represents the best fit to the emission which corresponds to an average emission measure EM = $6.9 \pm 2 \times 10^8$ cm$^{-6}$ pc and an effective blackbody area $A_{BB} = 1.9 \pm 0.5 \times 10^{-3}$ pc$^2$. These values were obtained assuming a free-free thermal flux of 6.4 Jy at 89 GHz. For a spherical geometry (i.e., $A_{BB} = \pi R^2$, and EM = $[4/3]n_e^2 R$) we find $R = 0.025 \pm 0.003$ pc and $n_e = 1.4 \pm 0.2 \times 10^5$ cm$^{-3}$. The value of the parameters agree within the errors with the parameters derived by GRvG from the longer wavelength data.

Since the H II region is optically thin at 89 GHz, we can use the observed flux to estimate the rate of ionizing photons ($N_i$) produced by the exciting source. For a flux of 6.4 Jy, $N_i = 1.0 \times 10^{49}$ s$^{-1}$, which is equivalent to the Lyman-continuum flux of an O6 ZAMS star (Panagia (1973). The total luminosity of such a star is $\sim 2 \times 10^5 L_\odot$. The infrared luminosity measured towards G34.3+0.2 is $L \sim 6 \times 10^5 L_\odot$ (Chini et al. 1987). As for other ultracompact H II regions (Wood et al. 1988), the total stellar luminosity inferred from radio continuum measurements is smaller than the infrared luminosity. The infrared "excess" is probably due in part to absorption of UV photons by dust. There may also be one or more additional younger stars in the core that have not yet ionized their surroundings.

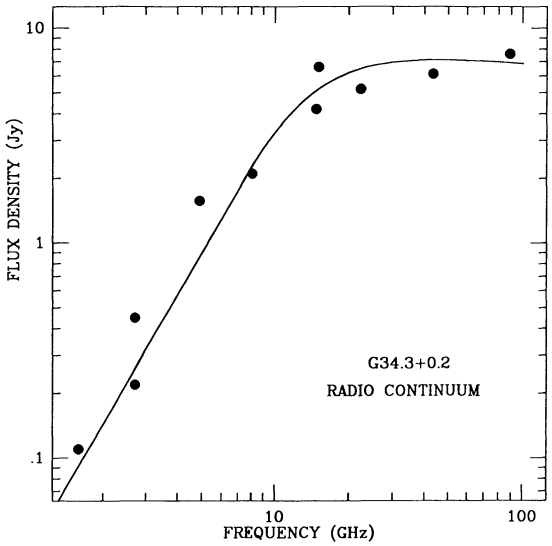


FIG. 1.—Radio fluxes measured toward G34.3+0.2 at frequencies from 1.6 to 89 GHz. A fit of the theoretical spectrum of a homogeneous H II region with electron temperature $T_e = 10{,}000$ K to the data (*solid line*) gives an emission measure EM = $6.9 \pm 2 \times 10^8$ cm$^{-6}$ pc and an effective blackbody area $A_{bb} = 1.9 \pm 0.5 \times 10^{-3}$ pc$^2$. References: Reid & Ho 1985; Turner et al. 1974; Wink, Altenhoff, & Mezger 1982; Benson & Johnston 1984; Garay et al. 1986; Garay et al. 1985; Matthews et al. 1977; Turner & Matthews 1984; Wood et al. 1988; this work.

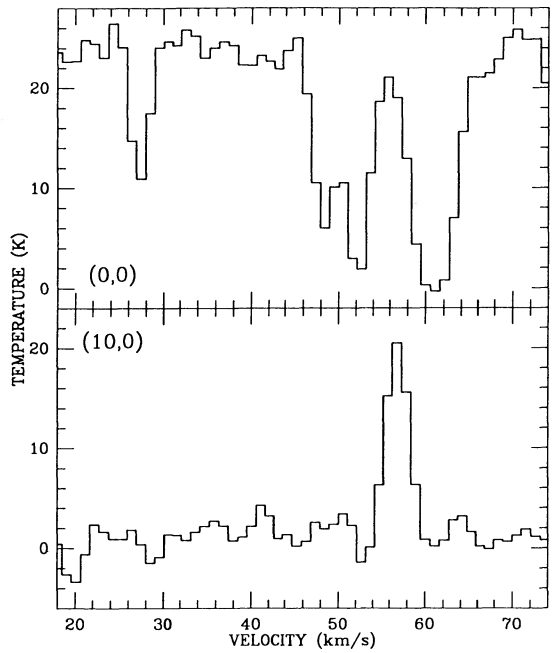


FIG. 2.—$HCO^+$ spectra toward the compact H II region G34.3+0.2. The offsets in arcseconds from the position of the compact H II region are indicated. The spectrum at (0, 0) shows absorption features at 27, $\sim$52, and 61 km s$^{-1}$, whereas the spectrum 10″ to the east, with no background continuum source, shows only one emission line at about 57 km s$^{-1}$.

### 3.2. *Molecular Line Emission toward G34.3+0.2*

#### 3.2.1. $HCO^+$

The $HCO^+(J = 1 \rightarrow 0)$ line toward G34.3+0.2 is detected in emission over $\sim$45″–50″. The peak brightness temperature observed is $T_B(HCO^+) \sim 25$ K. In addition, $HCO^+$ is detected in absorption against the compact continuum source. The profile, shown in Figure 2 (*top*), shows absorption features at 27, $\sim$52, and 61 km s$^{-1}$ toward the H II region; in contrast, a spectrum 10″ east of it (*bottom*), with no background continuum source, shows only one emission line at about 57 km s$^{-1}$. The absorption features will be discussed below. The $HCO^+$ emission morphology resembles half a disk with a mean radius of 24″ (0.45 pc) approximately centered on the compact H II region. In Figure 3 we compare $HCO^+$ maps, with and without the continuum (*left* and *right*). The maps were obtained integrating the emission over the velocity range 54–59 km s$^{-1}$. The presence of absorption features at 52 and 61 km s$^{-1}$ make the line emission distribution look "bean-shaped" with a depression at the position of the compact H II region. Matthews et al. (1987) observed the $HCO^+$ $J = 1 \rightarrow 0$ line toward the same region using the 20 m Onsala dish. Their $HCO^+$ map, with 40″ spatial resolution, shows a $HCO^+$ structure $\gtrsim 2'$ in extent. Evidence for undersampled extended ($\gtrsim$40″) $HCO^+$ emission is apparent in our $HCO^+$ maps as

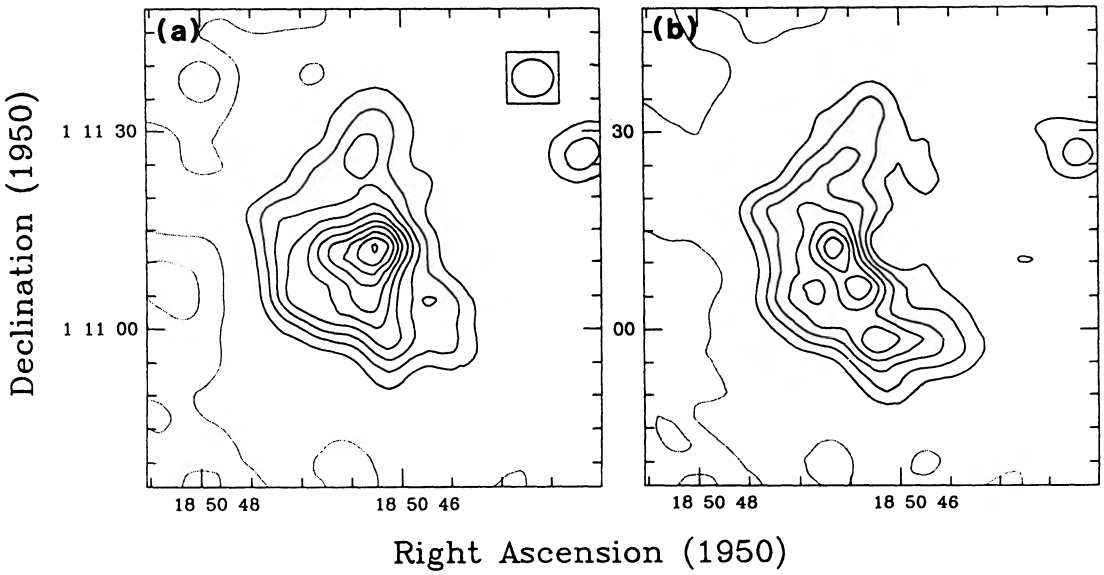


FIG. 3.—(*a*) Image of integrated $HCO^+$ $J = 1 \rightarrow 0$ and 3.4 mm continuum emission toward G34.3+0.2. The contour interval is 8.4 K km $s^{-1}$. The beam, 6".3 × 5".6, is shown in the upper right corner. (*b*) Image of integrated $HCO^+$ $J = 1 \rightarrow 0$ emission only.

negative dips. In Figure 4, we compare the single-dish $HCO^+$ spectrum shown in Matthews et al. (1987) paper (taken ~17" north of the compact H II region) with a Hat Creek spectrum at the same position obtained by convolving the channel maps with a 40" Gaussian beam. The brightness temperature in the Hat Creek spectrum is less than 50% that of the single dish indicating missing extended flux in the Hat Creek maps. The single-dish profile shows an emission component at approximately 65 km $s^{-1}$; this component must be smooth and extended and of low surface brightness since it is not seen in emission in the Hat Creek spectra. However, the Hat Creek $HCO^+$ profile toward the compact H II region (see Fig. 2) shows weak absorption up to 68 km $s^{-1}$ indicating that some

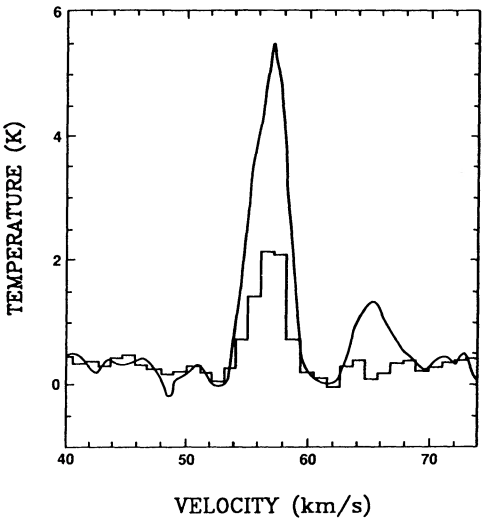


FIG. 4.—Superposition of a Hat Creek spectrum obtained by convolving individual channel maps with a 40" beam (histogram) with the single-dish spectrum obtained by Matthews et al. (1987) in the same position and a similar beam (*smooth line*). The interferometer detects less than 50% of the single-dish flux.

of the $HCO^+$ extended redshifted gas at 65 km $s^{-1}$ is in front of the compact H II region. Such gas must be dense [$n(H_2) \gtrsim$ few $10^4$ $cm^{-3}$] because it is detected in emission with the single antenna.

The location and morphology of the relatively compact $HCO^+$ core seen in emission in the Hat Creek maps suggests a spatial association with the ionized compact regions. Note, however, the radial velocity difference. The $HCO^+$ velocity centroid is 57 km $s^{-1}$, whereas the H41α radio recombination line velocity is 48.8 km $s^{-1}$.

To estimate a lower limit to the mass of the $HCO^+$ core we assume optically thin emission. In this case, the mass of the core can be obtained from the expression

$$M = 3 \times 10^{-14} \left(\frac{\langle S \rangle}{\text{Jy}}\right)\left(\frac{\Delta v}{\text{MHz}}\right)\left(\frac{A_{ul}}{\text{s}^{-1}}\right)^{-1}\left(\frac{v}{100\ \text{GHz}}\right)^{-1} \times \left(\frac{f}{0.1}\right)^{-1}\left(\frac{N}{\text{H}_2}\right)^{-1}\left(\frac{D}{\text{kpc}}\right)^2 M_\odot , \quad (1)$$

where $\langle S_v \rangle$ is the total flux averaged over $\Delta v$, $D$ is the distance to the source, $A_{ul}$ is the Einstein probability coefficient for spontaneous decay, $f$ is the fraction of molecules in the upper level of the observed transition, and $N/H_2$ is the fractional molecular abundance with respect to hydrogen. Assuming a fractional abundance $[HCO^+]/[H_2] = 2.3 \times 10^{-9}$ equal to the one in the Orion extended ridge (Blake et al. 1987, hereafter BSMP), and assuming $T_{ex} = T_B = 25$ K and local thermodynamic equilibrium (LTE), the measured total flux ($\langle S_v \rangle \Delta v$) of 55 Jy MHz yields a strict mass lower limit of 100 $M_\odot$.

A velocity gradient is present across the $HCO^+$ core. Figure 5 shows intensity maps of several velocity channels (the blue-shifted and redshifted absorption features are also seen in the maps). The spatial distribution of the $HCO^+$ emission changes with velocity; the gas at ~53 km $s^{-1}$ is located SW of the H II region and moves toward the NE as the velocity increases to ~59 km $s^{-1}$. The smooth change of position with velocity suggests that the detected gradient is due to rotation of the $HCO^+$ emitting core.

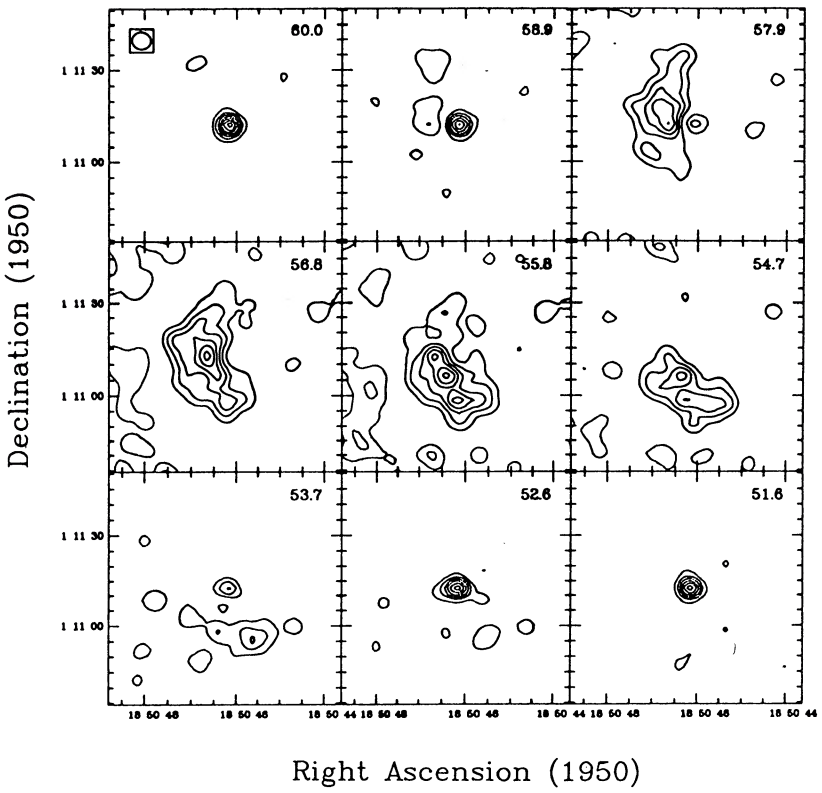


FIG. 5.—Channel maps of the $HCO^+(J = 1 \rightarrow 0)$ emission in G34.3+0.2. The contour interval is 3.3 K. The beam, 6″.3 × 5″.6, is shown in the upper left corner of the first map. The average LSR velocity corresponding to each map is printed in the upper right corner. The emitting region moves from the SW to NE as the velocity increases.

### 3.2.2. $H^{13}CN$

Emission from the $H^{13}CN(J = 1 \rightarrow 0)$ transition is detected over a region ~15″ in extent (0.3 pc). The peak in the emission maps is offset (~2″) east of the compact H II region. Spectra across the $H^{13}CN$ core are shown in Figure 6. The $F = 1$–1 redshifted hyperfine component seems to be partially absorbed by the foreground gas component at $V_{LSR} = 61$ km s$^{-1}$ seen also in the $HCO^+$ profile described above. The ratio measured between the other two hyperfine components, $F = 1$–0 and the $F = 2$–1, is 0.35 ± 0.05. Such ratio is large compared with the value of 0.2 expected if the components are in LTE and the emission is optically thin. The large line ratio is probably due to a substantial optical depth in the main, $F = 2$–1 component. Additional evidence for a significant optical depth comes from the $HC^{15}N$ to $H^{13}CN$ intensity ratio. The brightness temperature ratio of the $HC^{15}N$ line and the main hyperfine component of the $H^{13}CN$ line is 0.45; the value expected for optically thin lines is 0.27 assuming an abundance $[HC^{15}N]/[H^{13}CN]$ typical of molecular clouds of about 0.15 (Wannier 1980). The measured value of 0.45 suggests that the main hyperfine $H^{13}CN$ line has an optical depth greater than 1.

In contrast to the $HCO^+$ profile shown in Figure 2, the $H^{13}CN$ spectrum at the position of the compact H II region shows little absorption of the free-free continuum. We measure a peak brightness temperature $T_B(H^{13}CN) = 12 \pm 1$ K with $V_{LSR} \sim 57$ km s$^{-1}$ for the main component which varies smoothly across the source. The lack of absorption suggests that most of the $H^{13}CN$-emitting gas lies behind and to the side of the H II region.

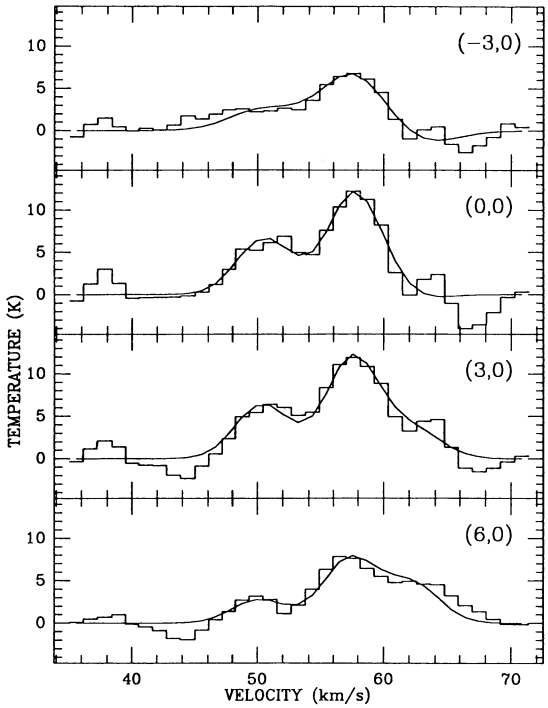


FIG. 6.—$H^{13}CN$ spectra across the molecular core in G34.3+0.2. The offset in arc seconds from the position of the compact H II region is indicated in the upper right-hand corner of each box. The line fits are also drawn with a solid line.

A nearly south-north velocity gradient across the $H^{13}CN$ core is suggested in position-velocity emission plots. In Figure 7 are shown the plots obtained from uniform-weighted maps for cuts at p.a. 5° and 95°. We measured a velocity shift of about 3 km $s^{-1}$ which corresponds to a gradient of 13 ± 6 km $s^{-1}$ $pc^{-1}$ over ~0.22 pc. The gradient will be discussed in § 4.3.

### 3.2.3. $HC^{15}N$

Emission from the $J = 1 \rightarrow 0$ $HC^{15}N$ transition was detected toward G34.3+0.2. The emitting source is unresolved in our uniformly weighted maps with 6″.5 × 5″.4 spatial resolution. The peak in the integrated map is offset to the east of the compact H II region by ~1″.5. Given the low abundance of the $HC^{15}N$ isotope of HCN, the $HC^{15}N$ emission is almost certainly optically thin and traces the gas components with the largest column density in the region. The $HC^{15}N$ emission is probably associated with the ultracompact core (size ~0.02–0.06 pc) studied by HWM, HLB, and GR which has a large temperature ($T_K \sim 225$ K) and hydrogen density [$n(H_2) \gtrsim 10^7$ $cm^{-3}$]. The $HC^{15}N$ spectrum obtained from the naturally weighted maps is shown in Figure 8. A Gaussian fit to the spectrum gives $T_B(HC^{15}N) = 5.4 \pm 0.5$ K, $\Delta V_{FWHM} = 6 \pm 0.7$ km $s^{-1}$, and $V_{LSR} = 56.4 \pm 0.3$ km $s^{-1}$.

The total flux measured toward the $HC^{15}N$-emitting region is 4.7 Jy MHz. Since the line is almost certainly optically thin,

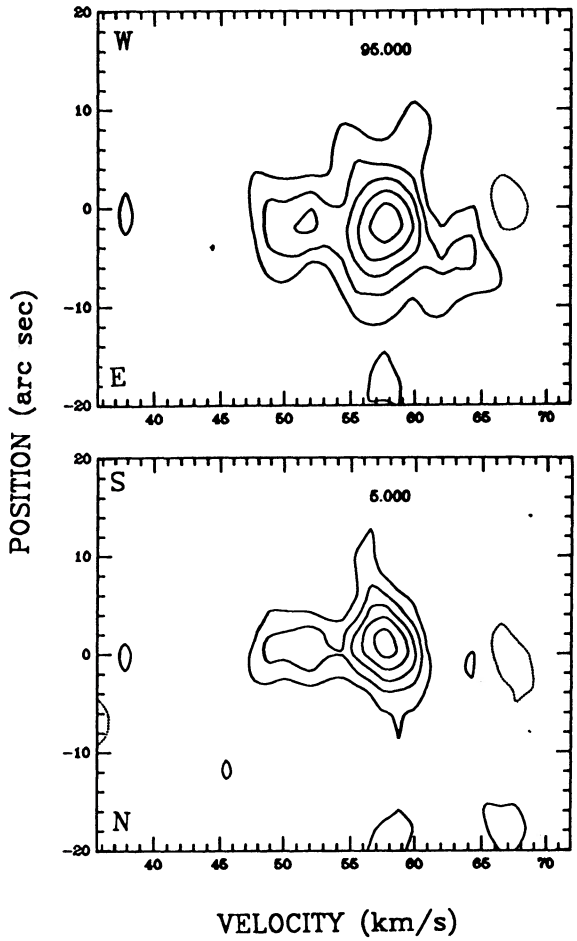


FIG. 7.—Position-velocity plots made from $H^{13}CN$ uniform-weighted maps. The plots show cuts at p.a. 5° and 95°. A velocity gradient is suggested in the SN direction.

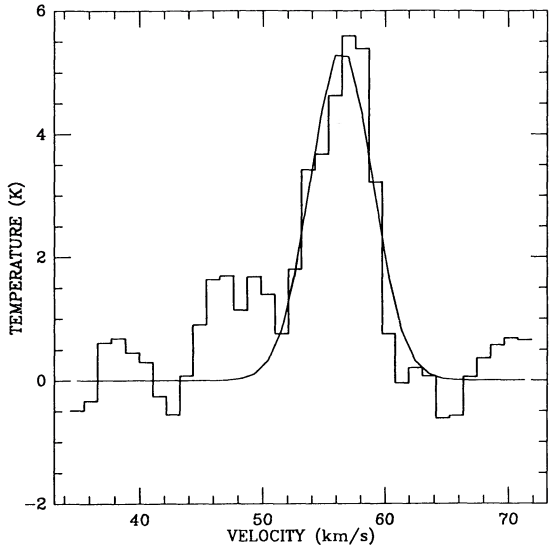


FIG. 8.—$HC^{15}N$ spectrum toward G34.3+0.2 obtained from naturally weighted maps. The Gaussian fit is drawn with a smooth solid line. The fit gives $T_B(HC^{15}N) = 5.4 \pm 0.5$ K, $\Delta V_{FWHM} = 6 \pm 0.7$ km $s^{-1}$, and $V_{LSR} = 56.4 \pm 0.3$ km $s^{-1}$.

we can estimate the mass in the region using equation (1) assuming LTE. The brightness temperature of the observed $HC^{15}N$ line sets a lower limit to the excitation temperature; however, the gas kinetic temperature and gas density in the region, as mentioned above, are very high [$T_K = 225 \pm 75$ K, $n(H_2) = 4 \times 10^7$ $cm^{-3}$], and therefore the excitation temperature of the $HC^{15}N$ transition is probably higher than 5.4 K. Assuming $T_{ex}(HC^{15}N) = 225$ K, the fraction $f$ of molecules in the $J = 1$ level is 0.027. For an abundance $[HCN]/[H_2] = 5 \times 10^{-9}$, equal to the one measured in the Orion ridge (BSMP), and $HCN/HC^{15}N = 273$ equal to solar (see, e.g., Wannier 1980), we obtain a mass of $2 \times 10^4$ $M_\odot$ in the compact source. The mass in such a small region ($\lesssim$0.06 pc) is unlikely to be so big, suggesting that it has been overestimated because of the HCN fractional abundance assumed.

A constraint on the mass of the gas in the compact region where $HC^{15}N$ is detected can be set from the upper limit on 3.4 mm continuum emission. In § 3.1 above, we estimated an upper limit of 1.6 Jy for the dust contribution to the 3.4 mm flux. If the ultracompact core in G34.3+0.2 is similar to the hot core in Orion, we can estimate an upper limit to the mass of the ultracompact core in G34.3+0.2. Orion's hot core has a flux of 0.25 Jy at 3.4 mm (Wright & Vogel 1985) and is 7.6 times closer than G34.3+0.2. Since the dust emission at 3.4 mm in G34.3+0.2 is no more than 6.4 times the flux from the Orion hot core, the mass is only ($M \propto$ flux × distance$^2$) ~ 370 times larger. The mass of the Orion hot core is 1–5 $M_\odot$ (Morris, Palmer, & Zuckerman 1980; Masson et al. 1984; Wright & Vogel 1985); therefore, the mass of the ultracompact core at G34.3+0.2 would be in the range 370–1850 $M_\odot$ which is more than 10 times smaller than the estimate above.

### 3.2.4. SO

Emission from the $(2_2 \rightarrow 1_1)$ transition of SO was detected toward G34.3+0.2. The emitting region is slightly resolved by our beam (6″.5 × 5″.4) indicating it is not as compact as the $HC^{15}N$ component. We set a rough upper limit ~0.07 pc for the size of the SO-emitting region. The SO spectrum and a Gaussian fit to the line are shown in Figure 9. The line param-

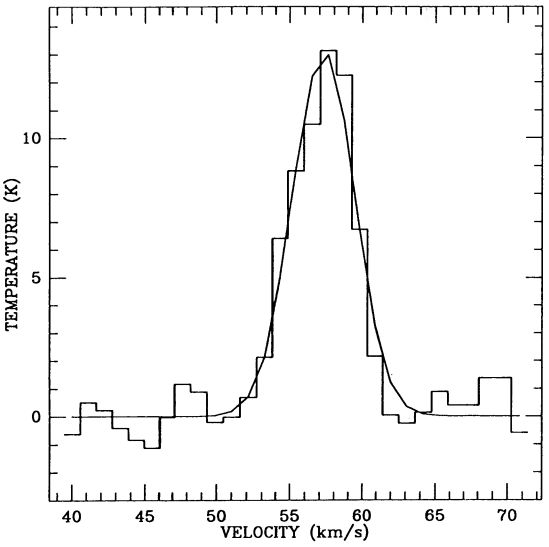


FIG. 9.—Plot of the SO spectrum toward G34.3+0.2 obtained from uniformly weighted maps. The best Gaussian fit, with parameters $T_B(\mathrm{SO}) = 13 \pm 0.6$ K, $\Delta V_{\mathrm{FWHM}} = 5 \pm 0.3$ km s$^{-1}$, and $V_{\mathrm{LSR}} = 57.3 \pm 0.1$ km s$^{-1}$, is also plotted.

eters are $T_B(\mathrm{SO}) = 13 \pm 0.6$ K, $\Delta V_{\mathrm{FWHM}} = 5 \pm 0.3$ km s$^{-1}$ and $V_{\mathrm{LSR}} = 57.3 \pm 0.1$ km s$^{-1}$. A map of the integrated emission is shown in Figure 10. The integrated SO map peaks $\sim 1''$ east of the compact H II region. As pointed out before, the $HC^{15}N$ and $H^{13}CN$ emission peaks are also 1″ to 2″ to the east. The observations by HLB with $\sim 1''$ resolution revealed that the ammonia ultracompact core lies on the eastern rim of the cometary H II region. Probably the offsets in the SO, $HC^{15}N$, and $H^{13}CN$ emission peaks are real and indicate the line of sight with the largest column density and temperature, in the direction of the ultracompact core.

A lower limit to the mass of the SO-emitting gas can be estimated from eq. (1). The total flux measured in the SO component is $\langle S \rangle \Delta v = 6.8$ Jy MHz. In LTE, the fraction of SO molecules in the $2_2$ level varies from 0.023 to 0.007 assuming the SO excitation temperature is in the range $T_{\mathrm{ex}}(\mathrm{SO}) = 60$–225 K. If we assume a fractional abundance $[\mathrm{SO}]/[\mathrm{H_2}] \lesssim 9.3 \times 10^{-10}$ equal to the limit derived for the Orion extended ridge by BSMP, the lower limit of the mass associated with the SO emission is 3000–9900 $M_\odot$ for $T_{\mathrm{ex}}(\mathrm{SO})$ between 60 and 225 K. Such a mass is larger than the limit of 1850 $M_\odot$ obtained above from the 3.4 mm dust emission. The large mass estimates indicate that the SO fractional abundance in the region is probably larger than the assumed value.

The SO maps show a shift in the peak emission as a function of velocity. Figure 11 shows position-velocity diagrams of the SO emission for cuts at 5° and 95°. The cut at 5° shows the gradient, whereas the cut at 95° does not, being perpendicular to the gradient. We measured the gradient from the position-velocity map and also from fitting Gaussians to the spectra obtaining $20 \pm 10$ km s$^{-1}$ pc$^{-1}$ over $0.2 \pm 0.1$ pc. The $HC^{15}N$ maps also suggest a gradient, but the gradient is less clear than in the SO maps because the lack of spatial resolution is more critical in this case. Note that the orientations of the velocity gradients are the same, within the errors, for the $HCO^+$-, $H^{13}CN$-, and SO-emitting sources.

### 3.3. $HCO^+$ *Absorption Features toward G34.3+0.2*

As mentioned in § 3.2.1, absorption features at 27, $\sim 52$ and 61 km s$^{-1}$ are observed in the $HCO^+$ spectrum taken toward

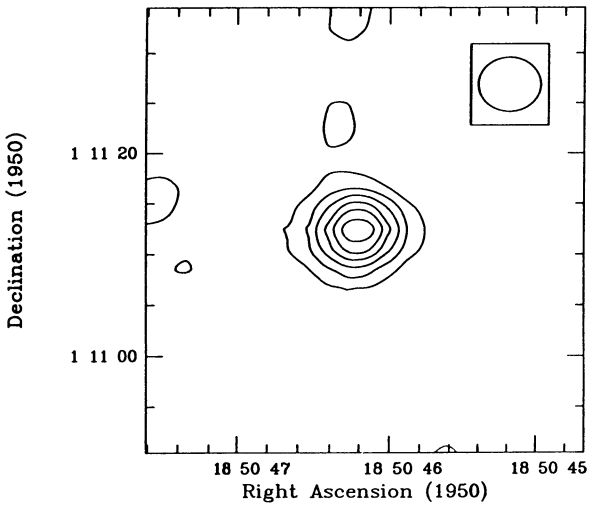


FIG. 10.—Integrated map of the SO($2_2 \rightarrow 1_1$) emission in G34.3+0.2. The contour interval is 9.5 K km s$^{-1}$. The beam, 6″.5 × 5″.4, is shown in the upper right-hand corner. The SO emission is barely resolved.

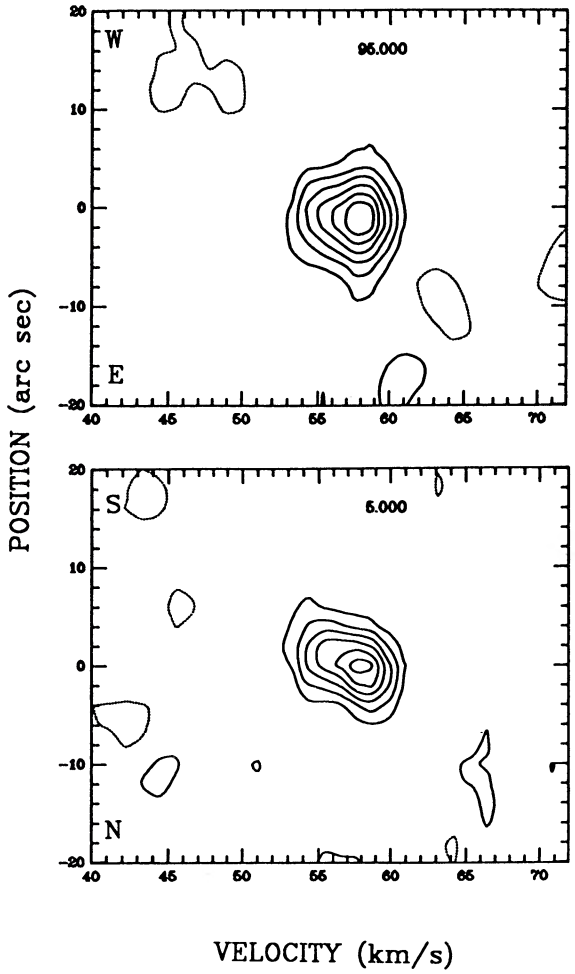


FIG. 11.—Position-velocity plots made from SO uniform-weighted maps. The plots show cuts at p.a. 5° and 95°. A velocity gradient is detected in the SN direction.

the compact H II region (see Fig. 2). In this section we describe the characteristics of each feature.

#### 3.3.1. *Absorption at* 27 km s$^{-1}$

The Hat Creek $HCO^+$ spectrum toward the compact H II region shows an approximately 14 K deep absorption at 27 km s$^{-1}$. The LSR velocity of this molecular component is very different from the velocity of the molecular gas seen in emission ($V_{LSR} \sim 57$ km s$^{-1}$). The difference in velocity indicates that the 27 km s$^{-1}$ cloud is probably not associated with G34.3+0.2. Using the rotation curve of the Galaxy derived by Brand (1986) we calculate a kinematic distance of 1.8 kpc for the cloud. The CO spectrum obtained toward G34.3+0.2 by Matthews et al. (1987) shows a low brightness emission line at 27 km s$^{-1}$ probably associated with the same component. This component seems to be an independent low-density ($n_{H_2} \lesssim 10^3$ cm$^{-3}$), cold cloud along the line of sight. The optical depth at the center of the line is 0.8 and the corresponding column density $N(HCO^+) = 1.1 \times 10^{12}$ cm$^{-2}$ for a $T_{ex} = 2.7$ K in the $HCO^+$ $J = 1 \rightarrow 0$ transition. Assuming an $HCO^+$ fractional abundance $\sim 2 \times 10^{-9}$, appropriate for quiescent clouds (see, e.g., BSMP), the corresponding hydrogen column density is $N[H_2] \sim 5.5 \times 10^{20}$ cm$^{-2}$.

#### 3.3.2. *Absorption at* 52 km s$^{-1}$

The $HCO^+$ spectrum at the position of the compact H II region shows also absorption in the velocity range from 46 to $\sim 54$ km s$^{-1}$. The absorption is deepest at 52 km s$^{-1}$. The LSR velocity of the molecular lines seen in *emission* toward G34.3+0.2 is $V_{LSR} \sim 57$ km s$^{-1}$. Therefore, the absorption feature is blueshifted with respect to the dense core seen in emission. Even though the measured peak optical depth of this line is $\sim 2.5$, the single-dish $HCO^+$ profile (Matthews et al. 1987) does not show any emission at these velocities. This indicates that the excitation temperature of the $HCO^+(J = 1 \rightarrow 0)$ transition is very close to 2.7 K and suggests that this molecular component has low molecular hydrogen density. Assuming a $T_{ex}(HCO^+) = 2.7$ K, we calculate an $HCO^+$ column density $N(HCO^+) = 6.0 \times 10^{12}$ cm$^{-2}$. The corresponding hydrogen column density is $N(H_2) = 3 \times 10^{21}$ cm$^{-2}$ for an $HCO^+$ fractional abundance of $2 \times 10^{-9}$ (BSMP).

We looked in the 21 cm H I surveys by Weaver & Williams (1974) and Shane (1971) for evidence of neutral hydrogen at 52 km s$^{-1}$ toward G34.3+0.2. We found an H I component in Shane's list at $l = 34.^\circ29$, $b = 0.^\circ18$ with $\sigma_b = 0.^\circ95$ which overlaps in position with G34.3+0.2. The associated velocity is 50.8 km s$^{-1}$ with a dispersion of 3.4 km s$^{-1}$ and a column density of $3 \times 10^{21}$ cm$^{-2}$. The Galactic coordinates, velocity centroid, and column density of this H I source suggest that it is associated with the low-density $HCO^+$ cloud seen in absorption. However, the $HCO^+$ absorption extends over a larger velocity range suggesting that it may have a contribution from an additional component. The $^{12}CO$ and $^{13}CO$ single dish profiles in the Matthews et al (1987) study with 30″ resolution, show emission in the velocity range where we detect the absorption (i.e., 46–54 km s$^{-1}$). Matthews et al. interpret the blueshifted CO emission as a flow produced by interaction of the compact H II region with the ambient medium. However, as discussed above, the blueshifted molecular gas at $\sim 52$ km s$^{-1}$ is likely to be associated with the extended ($\sigma_b \sim 0.^\circ95 \sim 50$ pc) H I component along the line of sight not directly associated with the H II region.

#### 3.3.5. *Absorption at* 61 km s$^{-1}$

The continuum emission from the compact H II region in G34.3+0.2 is completely absorbed at 61 km s$^{-1}$ by molecular gas along the line of sight (see the spectrum in Fig. 2). Absorption at 61 km s$^{-1}$ is also detected by GR and Keto et al. (1987b) in ammonia inversion lines, and by Matthews et al. (1987) in self-absorbed millimeter $HCO^+$, $^{12}CO$, and $^{13}CO$ single-dish spectra. Self-absorbed $^{13}CO$ profiles in the Matthews et al. study are detected over the whole region they mapped ($\sim$few pc; see their Fig. 9), and therefore, it is not yet clear what the total extent of the absorbing cloud is. Matthews et al. mention in their paper that the absorption feature in the $HCO^+$ spectrum is deeper toward the center of the core, suggesting that the dimension of the absorbing cloud is not much larger than the $HCO^+$ core they mapped with the Onsala 20 m telescope, i.e., a couple of parsecs.

The low brightness temperatures seen in the Matthews et al. $HCO^+$ single-dish profile and in our spectrum suggest a line excitation temperature close to 2.7 K. The low excitation of the gas is also evident from other transitions. Matthews et al. obtain an excitation temperature of 9 K from their $^{12}CO$ and $^{13}CO$ profiles. GR derive a rotational temperature of 18 K for the absorbing gas from observations of the (2, 2) and (1, 1) ammonia lines. The relatively larger temperature measured from the ammonia observations suggests that the ammonia is closer to the H II region. The gas density determination for the absorbing gas by Matthews et al. [$n(H_2) \sim 3 \times 10^3$ cm$^{-3}$] and GR ($10^4$ cm$^{-3}$) are more uncertain because the cloud diameter is unknown.

We argue that the 52 km s$^{-1}$ and the 61 km s$^{-1}$ absorption features are not part of a single, very broad feature but they are associated with different gas components. If we assume that such a broad gas component existed and laid uniformly in front of the "quiescent" $HCO^+$ core described above, then the excitation temperature of the background $HCO^+$-emitting gas would have to be unrealistically large over the whole $HCO^+$ core. In addition, other molecular tracers observed toward the H II region show only a narrow absorption feature at $\sim 61$ km s$^{-1}$ (GR; Keto et al. 1987b; Martín-Pintado et al. 1985). While no H I component at 61 km s$^{-1}$ appears in the Shane (1971) list of clouds, there is an H I gas component at the velocity of the 52 km s$^{-1}$ feature. The two $HCO^+$ features appear to originate from gas with different properties.

The absorbing gas moving at 61 km s$^{-1}$ may be either a nearby, probably interacting, foreground cloud or an envelope surrounding the core. If the absorbing gas is an envelope, the redshift in velocity indicates that it is collapsing toward the dense molecular core. In this picture, some or most of the detected emission in our $HCO^+$ spectra is the blueshifted inner edge of the envelope behind the H II region. The complex molecular line profiles toward the region indicate that detailed mapping of the extended cloud is necessary to study the distribution and kinematics of the absorbing gas in more detail.

## 4. DISCUSSION

### 4.1. *Models for the Cometary* H II *Region*

Various models have been suggested to explain the cometary morphology of the compact H II region in G34.3+0.2. Reid & Ho (1985) suggested that the brightness distribution observed in G34.3+0.2 could be produced if the star ionizing the gas moves relative to the molecular environment. Detailed modeling of this circumstance, intended to explain cometary H II

regions in general, has been done recently by van Buren et al. (1990) and Mac Low et al. (1991) who included the effects of a stellar wind in the gasdynamics. Their wind models can match the morphologies and brightness distribution of observed objects. In their first attempt to model the cometary H II region in G34.3+0.2 with a wind bow shock, van Buren et al. and Mac Low et al. assumed that the star is moving perpendicular to the line of sight at 10 km $s^{-1}$. Detailed comparison between the predicted and observed velocity field of the ionized gas and molecular gas, however, has not been made for this source.

Champagne models based on the expected evolution of H II regions have also been invoked to explain the "cometary" radio morphology of the compact H II region in G34.3+0.2. Tenorio-Tagle (1979) suggested that if an expanding H II region embedded in a molecular cloud encounters the edge of the cloud, the large pressure discontinuity at the boundary would lead to a rapid outward acceleration of the ionized material. Expansion velocities in excess of $v_{exp} \sim 30$ km $s^{-1}$ are possible in such "champagne flows." If a champagne model applies to G34.3+0.2 we expect to find the H II region at the *edge* of the molecular core.

The morphology of the $HCO^+$ core described in § 3 and shown in Figure 3 and, in particular, the asymmetry in the molecular gas distribution indicates that a density gradient exists along the western edge of the $HCO^+$ core where the compact H II region sits. The relative location of the molecular core and the H II region indicates, therefore, that the H II region is probably going through a champagne phase. Furthermore, as discussed in § 3 and also by GR, AG, and HLB, the densest molecular gas lies behind and to the side of the ultracompact H II region. Such a gas distribution is consistent with a champagne model where ionized gas escapes toward the observer presenting a velocity component blueshifted with respect to the molecular gas.

As discussed by van Buren et al. (1990), large gas velocities in champagne flow models, calculated for constant density clouds, are achieved in the vicinity of the nozzle. However, in G34.3+0.2 the velocity of the ionized gas in the bright head (or coma) of the cometary H II region is shifted by about 8 km $s^{-1}$ respect to the molecular lines in the core. Franco, Tenorio-Tagle, & Bodenheimer (1990) have studied the formation and expansion of H II regions in clouds with density stratification and find cases where the dense ionized gas in the cloud core will experience large acceleration and move at supersonic speed. Steep density gradients are present in the molecular core associated with G34.3+0.2 as seen from the emission distribution of various molecular lines and in particular by our high-resolution maps. GR describe the molecular density distribution in G34.3+0.2 as a function of distance by a power law $[n(H_2)/cm^{-3}] \sim 5.5 \times 10^4 \ (d/pc)^{-1.7 \pm 0.4}$. Steep density gradients exist in the cloud which could be driving motions in the dense ionized gas detected as a blueshift in the radio recombination lines.

In their bow shock model, Mac Low et al. (1991) use a stellar velocity of 10 km $s^{-1}$ to model the H II region in G34.3+0.2. In such a circumstance it is difficult to understand why the exciting star is observed in such a special location. The presence of other ultracompact H II regions and water masers nearby and the density structure of the core suggests that the $HCO^+$ core is the site where the star exciting the H II region was formed. If the molecular clump from which the exciting star formed had a speed of 10 km $s^{-1}$ when the free-fall collapse initiated, the star at its present evolutionary stage should not be found so closely associated with the parent molecular core. In $10^5$ yr, the star would have traveled about 1 pc.

The observations indicate that the cometary H II region in G34.3+0.2 is located at the edge of a dense molecular core and probably in a champagne phase. Detailed modeling needs to be done, however, to confirm whether such a model can reproduce the limb brightening observed in the high-resolution centimeter wavelength maps in addition to the observed kinematics.

### 4.2. *Abundance Enhancements and the Nature of the Ultracompact Source*

In § 3, we found that the hydrogen mass inferred for the gas in the ultracompact region where $HC^{15}N$ and SO emission is detected is implausibly large if we use the fractional abundances of HCN and SO measured for the Orion ridge, a typical interstellar region, by BSMP. The HCN and SO fractional abundances in the Orion ridge are probably low compared to those in the ultracompact region in G34.3+0.2 where $HC^{15}N$ and SO emission are detected.

We can estimate HCN and SO fractional abundances in the ultracompact source if we set limits to its total mass. Modeling the ultracompact core as a spherical source of radius of about 0.015 pc and density $7 \times 10^7$ $cm^{-3}$ implies a hydrogen mass of $M(H_2) = 48\ M_\odot$. If the SO and $HC^{15}N$ emission originates mostly in the ultracompact core, then from equation (1), assuming LTE and $T_{ex} = 225$ K, we obtain $M(SO) = 9.2 \times 10^{-6}\ M_\odot$ in SO. For the $HC^{15}N$-emitting gas we obtained $M(HCN) = 1.1 \times 10^{-4}\ M_\odot$ for a $[HCN]/[HC^{15}N]$ ratio of 273, equal to solar (see, e.g., Wannier 1980). For a total mass of 48 $M_\odot$ in the ultracompact core, the corresponding fractional abundances are $[SO]/[H_2] \sim 2 \times 10^{-7}$ and $[HCN]/[H_2] \sim 2.3 \times 10^{-6}$, with a [HCN]/[SO] ratio of $\sim 11$. Such SO fractional abundance is similar to the value estimated by BSMP in the Orion plateau source and the HCN fractional abundance is about 8 times the value in the Orion hot core or the plateau source. The [HCN]/[SO] ratio of $\sim 11$ in G34.3+0.2 is in between the values measured in the hot core ($\gtrsim 15$) and in the plateau ($\sim 2$).

The gas density and temperature required to excite the $HCO^+$ $J = 1 \rightarrow 0$ and $SO(2_2 \rightarrow 1_1)$ transitions are not so different; however, the spatial distribution of the molecular emission of the two species detected in G34.3+0.2 is quite different. The $HCO^+$ extends over $\sim 0.9$ pc whereas SO emission is detected only over $\lesssim 0.07$ pc. The different distribution of the $HCO^+$ and the SO emission must be due to an abundance difference. In the discussion above we concluded that the SO fractional abundance in G34.3+0.2 associated with the compact emitting source is $\sim 10^{-7}$. Therefore, the SO abundance is greater than "typical" $HCO^+$ fractional abundances $\sim 10^{-9}$. If the SO fractional abundance is $\sim 10^{-7}$ in the whole cloud, we should detect extended SO emission over the region where we detect $HCO^+$ unless the $HCO^+$ fractional abundance is also enhanced by more than a factor of 50–100. Even though an $HCO^+$ abundance enhancement is possible, it is more likely that the different spatial distribution of the two molecular species is a signature of a local SO as well as HCN abundance enhancement.

The two most studied massive star forming regions, Orion A and Sgr B2, show chemical inhomogeneities (see, e.g., Welch 1988; Goldsmith et al. 1987). Our results on G34.3+0.2 and similar results obtained in recent molecular line studies of other massive star-forming regions (e.g., Rudolph et al. 1990)

indicate that such chemical inhomogeneities are a common phenomenon in these active regions. In particular, compact SO sources are detected in the star-forming regions W49, W51 and Sgr B2 (W. J. Welch, private communication; Rudolph et al. 1990, and J. E. Carlstrom, private communication), and in the three cases they are closely associated with molecular outflows. An additional well-known example of an outflow with an SO compact source is Orion where the SO emission originates mostly in a region (size $\lesssim 0.05$ pc; Plambeck et al. 1982) which apparently outlines the boundary of the cavity cleared by the wind from IRc2.

Relative abundance enhancements of SO and other silicon and sulfur species may be expected in an oxygen-rich environment (see discussion in BSMP). To explain the compact SO sources associated with outflows mentioned above, Welch (1988) suggested that the required oxygen-rich environment is created when grain mantles and some grains are destroyed in the interaction of a protostellar wind with the ambient dense molecular gas. In G34.3+0.2, the presence of a strong wind or molecular flow in the region is suggested by the velocity range observed in the $H_2O$ maser emission which goes from 45 to 85 km s$^{-1}$ (Downes et al. 1979). The center of the maser emission coincides within the errors with the position of the ultracompact source. It is possible then, that the SO emission is also related to an outflow source produced by a young object embedded in the ultracompact core. Given the temperature reported for the ultracompact core of $\sim 225$ K, it cannot be unambiguously identified with a self-luminous object; the high temperature can be obtained by heating from the star ionizing the cometary H II region assuming it has a bolometric luminosity of $\sim 6 \times 10^5$. However, recent 0".3 resolution ammonia observations by Keto et al. (1992) find an unresolved source with a brightness temperature $> 300$ K. Such a limit in the brightness temperature suggests the presence of a self-luminous young object in the ultracompact core (see Keto et al. 1992) which could be producing an outflow traced in our observations by its interaction with the ambient medium, that is, by the enhancement of SO and HCN abundances.

### 4.3. *Velocity Gradients in the Molecular Cloud*

In § 3 we showed that velocity shifts across the molecular core are present at various scales. For the $HCO^+$ core we measure a velocity gradient of $5 \pm 1$ km s$^{-1}$ pc$^{-1}$ over $\sim 0.9$ pc. The smooth shift in position of the emitting gas distribution with velocity suggests that rotation of the molecular core is producing the gradient with rotation axes at $110° \pm 25°$. However, the limited spectral and spatial resolution does not allow us to rule out other possibilities, for example that two clouds, one in the SW and one in the east, are interacting. It is worth noting that large velocity gradients have been observed in other collapsed cores associated with massive young stars (see, e.g., Zheng et al. 1985; Keto, Ho, & Haschick 1987a; Carral et al. 1992).

In addition a south-north (SN) gas velocity gradient is suggested in the $H^{13}CN$ position velocity maps shown in Figure 7 which we estimate to be about $13 \pm 6$ km s$^{-1}$ pc$^{-1}$ over 0.22 pc. The SO emission also indicates the presence of a SN velocity shift across the ultracompact source of about $20 \pm 10$ km s$^{-1}$ pc$^{-1}$ over $\sim 0.2 \pm 0.1$ pc. Such gradient could also be interpreted as rotation since the direction of the angular velocity vector measured for the three structures is the same within the errors. If this is the case, then the coincidence in axis of rotation suggests that the SO, $HC^{15}N$, $H^{13}CN$, and $HCO^+$ emission are tracing different scales of a single cloud which rotates differentially. However, the gradient observed in the barely resolved SO source could be tracing different kinematics, like a tilted expanding (or contracting) flattened structure similar to the one observed in Orion (Plambeck et al. 1982). Maps with arcsecond resolution of the SO and $HC^{15}N$ emission will be necessary to resolve the spatial distribution of the gas and therefore decide which one of the possible models explains the observed velocity gradient in the compact SO source.

### 4.4. *A Model for Large-Scale Cloud Collapse in G34.3+0.2*

As mentioned in § 3, one possible explanation for the $HCO^+$ absorption feature at 61 km s$^{-1}$ (see Fig. 2) is the presence of a molecular envelope collapsing toward the dense molecular core. We construct a simple model of inside-out collapse on the entire G34.3+0.2 core (Shu 1977; Welch et al. 1987; Rudolph et al. 1990), and compare the predicted absorption spectrum with the 61 km s$^{-1}$ feature of Figure 2. An inspection of Figures 2, 6, 8, and 9 suggest that the systemic velocity for the region is between 57 and 58 km s$^{-1}$. In this model we interpret emission over 53–58 km s$^{-1}$ as the blueshifted emission from material infalling behind the continuum source. The foreground collapsing material falling onto the core is seen in absorption against the continuum source. We use the model, discussed in some detail by Rudolph et al. (1990), in which gas is infalling in the inner regions approximately in free fall. The dotted curve of Figure 12 shows the predicted model absorption. In the model, the outer collapse envelope is at 3.4 pc. A thousand solar masses of material have already fallen onto the core with an equal amount still infalling. The core onto which material is falling has a radius of 0.5 pc, as suggested by the emission map of Figure 3, and the spherical collapse is centered at 0.1 pc east of the continuum peak at the center of the $HCO^+$ emission. The intrinsic velocity spread is 2.0 km s$^{-1}$, the molecular hydrogen density is $2 \times 10^3$ cm$^{-3}$ at a radius of 0.5 pc, and the fractional abundance of $HCO^+$, which gives the best fit is $4 \times 10^{-9}$. The predicted absorption, covering the range 59–64 km s$^{-1}$ and shown by the dotted curve in Figure 12, agrees well with the observed 61 km s$^{-1}$ absorption feature.

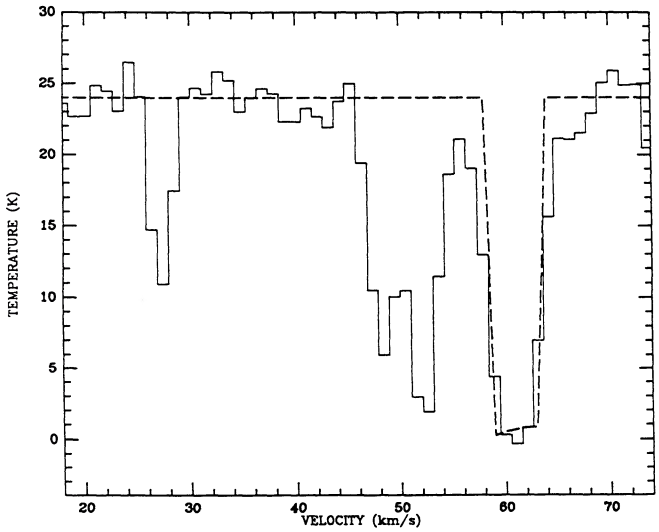


FIG. 12.—$HCO^+$ spectrum toward the compact H II region G34.3+0.2. The dashed line corresponds to the absorption profile predicted by the large-scale collapse model for the region discussed in § 4.4.

Thus one viable interpretation of the 61 km $s^{-1}$ absorption feature is indeed that it represents the collapse onto the entire G34.3+0.2 core. This large-scale collapse onto an entire core provides the means for synchronizing the star formation in an entire stellar association.

## 5. CONCLUSIONS

High-resolution observations of the molecular core in the star-forming region G34.3+0.2 are presented. Maps at 6″ resolution of emission and absorption of the $J = 1 \rightarrow 0$ transitions of $HCO^+$, $H^{13}CN$, $HC^{15}N$, and of the $2_2 \rightarrow 1_1$ transition of SO were obtained. In addition, a map of the 3.4 mm continuum emission from the compact H II component was obtained. The measured 3.4 mm flux requires that a Lyman-continuum flux equivalent to an O6 ZAMS star ionizes the ultracompact ("cometary") H II region.

The $HCO^+$ emission toward G34.3+0.2 traces a warm ($T_K \gtrsim 25$ K) molecular core about 0.9 pc in size. Emission from $H^{13}CN$ is detected over $\sim 0.3$ pc. The cometary H II region lies near the edge of the molecular core. The blueshift of the radio recombination lines with respect to the molecular emission suggests that gas from the H II region is accelerated in a champagne flow caused by a steep gradient in the ambient gas density. A velocity gradient of $\sim 5 \pm 1$ km $s^{-1}$ $pc^{-1}$, consistent with rotation, is detected across the $HCO^+$ molecular core. The position angle of the rotation axes is $110° \pm 25°$.

The SO and $HC^{15}N$ emissions detected in G34.3+0.2 originate in a small region ($\lesssim 0.07$ pc) located at the eastern edge of the compact H II region. The SO and HCN fractional abundances in this source appear to be enhanced locally. The compact SO source, high-velocity $H_2O$ masers in the region as well as the abundance enhancements may be associated with an outflow source produced by a young obscured object. A velocity gradient $\sim 20 \pm 10$ km $s^{-1}$ $pc^{-1}$ is detected across the compact source. The velocity gradient could be associated with an expanding and/or rotating flattened structure.

Three absorption features were detected against the compact continuum source in the $HCO^+$ spectrum. Two of them, at velocities of 27 and 52 km $s^{-1}$, appear to be clouds along the line of sight not associated with the dense $HCO^+$ core. The third component, at 61 km $s^{-1}$, is redshifted with respect to the core LSR velocity of $\sim 57$ km $s^{-1}$ and is apparently associated with the core. The absorbing gas may be part of an envelope surrounding the warm core and collapsing upon it, or alternatively, a foreground cloud moving toward the dense core and probably interacting with it.

P. Carral would like to thank Mel Wright for his advice on reducing the data. This work was supported by NSF grant AST87-14721. P. Carral also received support from a ZONTA Amelia Earhart Fellowship and from the National University of Mexico.

## REFERENCES

Andersson, M. 1985, in ESO-IRAM-Onsala Workshop on (Sub)millimeter Astronomy, ed. P. A. Shaver & K. Kjar (Garching: ESO), 353
Andersson, M., & Garay, G. 1986, A&A, 167, L1 (AG)
Benson, J. M., & Johnston, K. J. 1984, ApJ, 277, 181
Blake, G. A., Sutton, E. C., Masson, C. R., & Phillips, T. G. 1987, ApJ, 315, 621 (BSMP)
Brand, J. 1986, Ph.D. thesis, Leiden University.
Carral, P., Terebey, S., Turner, J. L., & Ho, P. T. P. 1992, in preparation
Carral, P., Welch, W. J., & Wright, M. C. H. 1997, Rev. Mexicana Astron. Af., 14, 506
Chini, R., Krügel, E., & Wargau, W. 1987, A&A, 181, 378
Downes, D., Genzel, R., Moran, J. M., Johnston, K. J., Matveyenko, L. I., Kogan, L. R., Kostenko, V. I., & Rönnäng, B. 1979, A&A, 79, 233
Forster, J. R., Caswell, J. L., Okumura, S. K., Hasegawa, T., & Ishiguro, M. 1990, A&A, 231, 473
Franco, J., Tenorio-Tagle, G., & Bodenheimer, P. 1990, ApJ, 349, 126
Garay, G., Reid, M. J., & Moran, J. M. 1985, ApJ, 289, 681
Garay, G., & Rodríguez, L. F. 1990, ApJ, 362, 191 (GR)
Garay, G., Rodríguez, L. F., & van Gorkom, J. H. 1986, ApJ, 309, 553 (GRvG)
Gaume, R. A., & Mutel, R. L. 1987, ApJS, 65, 193
Goldsmith, P. F., Snell, R., Hasegawa, T., & Ukita, N. 1987, ApJ, 314, 525
Heaton, B. D., Little, L. T., & Bishop, I. S. 1989, A&A, 213, 148 (HLB)
Heaton, B. D., Matthews, N., Little, L. T., & Dent, W. R. F. 1985, MNRAS, 217, 485
Henkel, C., Wilson, T. L., & Mauersberger, R. 1987, A&A, 182, 137 (HWM)
Keto, E. R., Ho, P. T., & Haschick, A. D. 1987a, ApJ, 318, 712
Keto, E. R., Ho, P. T., & Reid, M. J. 1987b, ApJ, 323, L117.
Keto, E. R., et al. 1992, in preparation.
Martín-Pintado, J., Wilson, T. L., Gardner, F. F., & Henkel, C. 1985, A&A, 142, 131
Masson, C. R., et al. 1984, ApJ, 283, L37
Mac Low, M.-M., van Buren, D., Wood, D. O. S., & Churchwell, E. 1991, ApJ, 369, 395
Matthews, H. E., Goss, W. M., Winnberg, A., & Habing, H. J. 1977, A&A, 61, 261
Matthews, N., Little, L. T., Macdonald, G. H., Andersson, M., Davies, S. R., Riley, P. W., Dent, W. R. F., & Vizard, D. 1987, ApJ, 184, 284
Morris, M., Palmer, P., & Zuckerman, B. 1980, ApJ, 237, 1
Panagia, N. 1973, AJ, 78, 929
Plambeck, R. L., Wright, M. C. H., Welch, W. J., Bieging, J. H., Baud, B., Ho, P. T. P., & Vogel, S. N. 1982, ApJ, 259, 617
Reid, M. J., & Ho, P. T. P. 1985, ApJ, 288, L17
Rudolph, A., Welch, W. J., Palmer, P., & Dubrulle, B. 1990, ApJ, 363, 528
Shane, W. W. 1971, ApJS, 4, 315
Shu, F. H. 1977, ApJ, 214, 488
Tenorio-Tagle, G. 1979, A&A, 71, 59
Turner, B. E., Balick, B., Cudaback, D. D., Heiles, C., & Boyle, R. J. 1974, ApJ, 194, 279
Turner, B. E., & Matthews, H. E. 1984, ApJ, 277, 164
van Buren, D., Mac Low, M.-M., Wood, D. O. S., & Churchwell, E. 1990, ApJ, 353, 507
Wannier, P. G. 1980, ARA&A, 18, 399
Weaver, H., & Williams, D. R. W. 1974, A&AS, 171
Welch, W. J. 1988, Ap. Letters Comm., 26, 181
Welch, W. J., Drehrer, J. W., Jackson, J. M., Terebey, S., & Vogel, S. N. 1987, Science, 238, 1550
Wink, J. E., Altenhoff, W. J., & Mezger, P. G. 1982, A&A, 108, 227
Wood, D. O. S., Handa, T., Fukui, Y., Churchwell, E., Sofue, Y., & Iwata, T. 1988, ApJ, 326, 884
Wright, M. C. H., & Vogel, S. N. 1985, ApJ, 297, L11
Zheng, X. W., Ho, P. T. P., Reid, M. J., & Schneps, M. H. 1985, ApJ, 293, 522